American Mineralogist, Volume 67, pages 926–936, 1982

Orientation of phase and domain boundaries in crystalline solids

MICHAEL E. FLEET

Department of Geology
University of Western Ontario
London, Ontario, Canada N6A 5B7

Abstract

Minimization of interfacial energy is the dominant factor controlling the shape and orientation of crystalline precipitates and replacement products in minerals. The dimensional misfit of strain-free lattices at a phase boundary is directly related to interfacial energy and its minimization provides a convenient criterion for calculating interface orientation. The contribution of anisotropic elasticity is relatively insignificant except when the lattice misfit is essentially isotropic.

The existing lattice-misfit theory of Robinson and coworkers for two-dimensional lattices and its application to chain-silicate mineral systems is reviewed, and extended to both coincident and optimal phase boundaries. By recognizing that coincident and optimal phase boundaries have indices (*hkl*) common to both lattices, a generalized lattice-misfit theory for three-dimensional lattices is developed and applied to feldspar mineral systems. For optimal boundaries, structural continuity across an interface may be improved by local coherency stresses and dislocations. Discrepancies with observed orientations arise from topological constraints and the decrease in specific surface area with coarsening.

Introduction

The shape and orientation of crystalline precipitates is theoretically dependent on a variety of complexly interrelated factors, the principal ones being structural (or topological) constraints, diffusion, minimization of interfacial energy and precipitate size (or specific surface area). Recent studies suggest that minimization of interfacial energy is the dominant controlling factor when the precipitate phase has a definite crystallographic relationship with the matrix phase (Cahn, 1968; Bollman and Nissen, 1968; Robinson, Jaffe, Ross and Klein, 1971; Willaime and Brown, 1974; Jaffe, Robinson and Tracy, 1975; Robinson, Ross, Nord, Smyth and Jaffe, 1977; Fleet, Bilcox and Barnett, 1980; Fleet, 1981). Such crystallographically oriented precipitates most commonly occur in the form of geometrically-shaped inclusions with a preferred shape orientation. Equidimensional, rounded inclusions (spheres) frequently have an oriented zonal distribution within the matrix.

In the present context, interfacial energy includes the Helmholtz free energy of the interface atomic structure *and* the energy required to establish and maintain that structure. For planar interfaces, *variation* in the Helmholtz free energy is largely dependent on the degree of structural correspondence between the two related phases (which simplistically may be equated with dimensional misfit of the two lattices). Dislocations, stacking faults, and the (three-dimensional) elastic strain energy required to establish and maintain the interface structure raise the total free energy of the system and therefore must be included in the interfacial energy.

At the present time it is clearly not possible to make meaningful calculations of interfacial energy and thereby quantitatively to account for the morphology of crystalline intergrowths. Hence attention has been directed to establishing criteria that either are related to interfacial energy or directly contribute to it, and which may be applied in a more straightforward manner. Opinion is divided between the dimensional misfit of the strain-free lattices (lattice misfit, Bollmann, 1967; 1970; Bollman and Nissen, 1968; Robinson *et al.*, 1971; 1977; Jaffe *et al.*, 1975; Fleet *et al.*, 1980; Fleet, 1981) and the elastic strain energy required to bring the two lattices to coherence at the interface (coherent elastic strain energy, Cahn, 1968; Willaime and Brown, 1974).

In this paper, the existing lattice-misfit theory for two-dimensional lattices is extended to three-dimensional lattices. The generalized theory is ap-

0003–004X/82/0910–0926$02.00

plied to feldspar mineral intergrowths, and the relative importance and interrelation of lattice misfit and coherent elastic strain energy are critically discussed.

Two-dimensional lattice misfit

Theory

Following Robinson *et al.* (1977), the conditions under which two plane lattices are coincident along a common line (or lines) are quite evident from inspection of Figure 1. **R** is a lattice vector of magnitude r to the point (x,y) in X,Y lattice space, and a, b, and γ are unit-cell parameters. The present theory is only concerned with comparison of vectors to equivalent points in the two lattices, and it is convenient to normalize lattice coordinates relative to y. Thus, $x = x_1 = x_2$; $y = y_1 = y_2 = 1$. For lattice 1:

$$r_1^2 = (a_1x)^2 + b_1^2 - 2a_1xb_1\cos(180 - \gamma_1),$$

and so on. When $\mathbf{R}_1$ and $\mathbf{R}_2$ have a common origin and the same orientation, the misfit between the two lattices in the direction of $\mathbf{R}_1$, $\mathbf{R}_2$ is given by:

$$(r_1^2 - r_2^2)/r_1^2 = [(a_1^2 - a_2^2)x^2 + 2(a_1b_1\cos\gamma_1 - a_2b_2\cos\gamma_2)x + (b_1^2 - b_2^2)]/[a_1^2x^2 + 2(a_1b_1\cos\gamma_1)x - b_1^2]$$

or

$$\Delta r^2/r_1^2 = (r_1^2 - r_2^2)/r_1^2 = (Ax^2 + Bx + C)/A_1x^2 + B_1x + C_1) \quad (1)$$

where, $A = a_1^2 - a_2^2$, $B = 2(a_1b_1\cos\gamma_1 - a_2b_2\cos\gamma_2)$, $C = b_1^2 - b_2^2$, $A_1 = a_1$, $B_1 = 2a_1b_1\cos\gamma_1$, $C_1 = b_1$.

When $(\Delta r^2/r_1^2) = 0$ the two lattices are coincident along a common line through $(x,1)$, with

$$x = [-B\pm(B^2 - 4AC)^{1/2}]/2A \quad (2)$$

Since real solutions of equation (2) are limited by $4AC < B^2$, lines of coincidence are restricted to specific combinations of unit-cell parameters. When $4AC < B^2$ there are *two* (non-equivalent) orientations of coincidence, and when $4AC = B^2$ there is just one. For orthogonal lattices, the requirement for two (symmetry-related) lines of coincidence is simply $-(b_1^2 - b_2^2)/(a_1^2 - a_2^2) > 0$, or $b_1 > b_2$ with $a_2 > a_1$, *etc.*

Lattices oriented to coincidence along a common line do not necessarily have common lattice points (except for the origin). In general, points of perfect registry of the two lattices [$(x,1)$, $(2x,2)$, *etc.*] are cosets of the lattices belonging to an equivalent class of points common to both lattices (Bollmann, 1970). If the two lattices are imagined to be juxtaposed along a line of coincidence, they are only in continuity *along* their common boundary line. There is continuity of lattice rows across the boundary, but the two lattices remain incoherent to diffraction.

The angle of inclination (Θ) of the boundary line to the nearest rational lattice direction ([10] in Fig. 1) is:

$$\Theta_1 = \cos^{-1}[(r^2 + (xa_1)^2 - b_1^2)/2xa_1r], \quad (3)$$

and the associated lattice rotation (ξ) required to achieve coincidence is:

$$\xi = [10]_1 \wedge [10]_2 = \Theta_2 - \Theta_1. \quad (4)$$

For $4AC > B^2$ a line of coincidence does not exist. However, the misfit between two lattices along a common equivalent line still varies with line orientation. The orientation which minimizes the misfit (the optimal orientation) is obtained by differentiation of equation 1, which gives:

$$(AB_1 - A_1B)x^2 + 2(AC_1 - A_1C)x + (BC_1 - B_1C) = 0. \quad (5)$$

The point $(x, 1)$ in Figure 1 then defines the optimal boundary between two plane lattices for which $4AC > B^2$. Boundary orientation and associated lattice rotation are calculated as in coincident–boundary theory.

Application to intergrowths of chain-silicate minerals

The two-dimensional lattice theory has direct application to the orientation of intergrowths between phases with monoclinic and other orthogonal space lattices when the translation distances along the common third axis (the unique axis of monoclinic lattices) are very similar. Figure 1 then becomes an orthogonal projection down the common axis of the two lattices for two intergrown phases.

The two-dimensional theory accurately reproduces the two observed orientations and associated lattice rotations of the lamellar phase in two-phase intergrowths of monoclinic pyroxenes (augite–pigeonite) and monoclinic amphiboles (tremolite–cummingtonite and hornblende–cummingtonite; Robinson *et al.*, 1971, 1977; Jaffe *et al.*, 1975), and of rod-like inclusions of magnetite (cubic) in

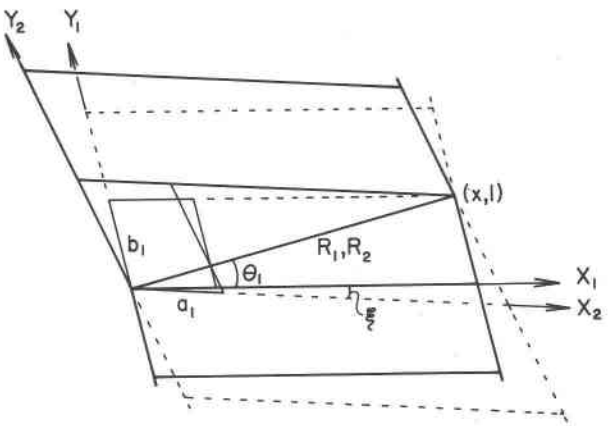

Fig. 1. Two plane lattices oriented to coincidence along a common boundary line: $\mathbf{R}_1\mathbf{R}_2$, coincidence vectors; θ, boundary line orientation; ξ, lattice rotation.

augite (Fleet *et al.*, 1980). When the effect of temperature and pressure of intergrowth formation on the unstrained unit–cell parameters is taken into account, the agreement between the calculated and observed data is only limited by experimental error. The orientation of magnetite in augite is particularly sensitive to temperature, and the predicted temperatures of magnetite precipitation agree well with those indicated by petrological evidence (Fleet *et al.*, 1980).

The *b* unit–cell parameters (unique axis Y) of these pairs of intergrown minerals are very similar, and only small stresses would be required to strain the lattices of the juxtaposed phases to be coincident in two-dimensions *at* the phase boundary. However, the phase-boundary calculations are not predicated on this assumption. For each intergrowth the relative difference in the *b* parameters is so small that it does not result in a significant component of phase boundary orientation outside of the *a*,*c* plane. This is confirmed by calculations with the three-dimensional lattice theory discussed below.

Although the two lattices in each of these pairs of intergrown minerals remain completely incoherent to diffraction, lattice rotation allows the related crystal structures to be "continuous" along the phase boundary plane *without* introducing elastic strain. Thus interfacial energy is minimized. For intergrowths of essentially isomorphous phases, the interface atomic structure will be generally similar to the related crystal structures. In contrast, the interface structure of augite–magnetite intergrowths must be a hybrid of two quite distinct chemistries and crystal structures. In all cases however, the degree of structural continuity permitted by the interface structure is sufficient to cause the interfacial energy to be minimized.

Robin (1974; 1977) has used the Mohr circle construction to calculate the stress-free strain ellipsoid and phase boundary orientation for intergrowths which may be reduced to two-dimensional lattice problems. This graphical method is based on the assumption that the strain of the interaxial angle (*e.g.*, $\gamma_1 - \gamma_2$) makes a linear contribution to the shear strain. Although this assumption may not be valid in all cases (*e.g.*, when $\gamma_1 = \gamma_2 \neq 90°$), the calculated data for chain silicate and alkali feldspar intergrowths (Robin, 1974; 1977; Tullis and Yund, 1979) do appear quite meaningful. However, for calculation of phase boundary orientation alone, the Mohr circle method of Robin is superseded by the theory of Robinson *et al.* (1977; represented by equations 1, 2, 3, and 4) for coincident boundaries and by equation 5 for optimal boundaries.

Three-dimensional lattice misfit

Theory

When the construction in Figure 1 is considered as an orthogonal projection down a common axis (Fig. 2), it becomes clear that the plane of coincidence of the two lattices passing through $(x,1,0)$ is actually parallel to the crystallographic plane $(\bar{h}10)$, where $h = 1/x$. Furthermore, intercepts on the reference axes, normalized to $0B_1 = b_1$, $0B_2 = b_2$, result in lines in the projection (A_1B_1, A_2B_2) which are identical in magnitude and orientation to the coincidence vector, **R**. Thus the two lattices can be placed in coincidence in the lattice plane represented by A_1B_1 by simply translating lattice 2 along the line B_2B_1.

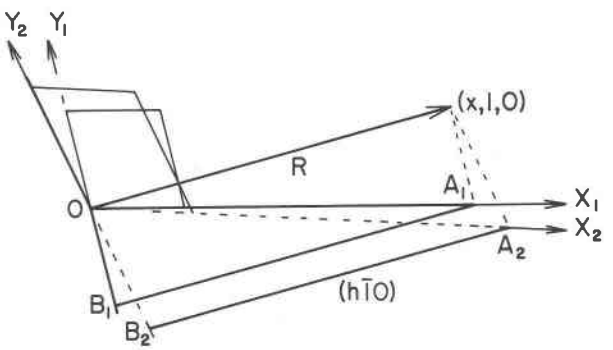

Fig. 2. Equivalence of coincidence vector **R** and normalized intercepts A_1B_1,A_2B_2.

The equivalence of **R** and A_1B_1,A_2B_2 forms the basis of the present three-dimensional optimal phase–boundary theory and leads to the statement of a crystallographic law: that coincident and optimal phase boundaries have indices (*hkl*) common to both crystal lattices. The points of intersection of an (*hkl*) plane with the three reference axes define a reference triangle (Fig. 3) in each lattice. The sides of the reference triangle are normalized by setting 0B = *b*. For intergrown phases which are isomorphs, and which therefore have topological equivalence for unit translations along crystallographic axes, the corners of the reference triangles are equivalent points in the two juxtaposed structures. Thus if it were possible for their lattices to have a common plane of coincidence, the crystal structures of two intergrown isomorphous phases would be continuous along their common phase boundary.

In fact, it is not possible for two different strain-free triclinic lattices to have a common plane of coincidence. They may have common *lines* of coincidence. Indeed each of the sides of the reference triangle may perhaps be separately and independently brought to coincidence by an appropriate lattice rotation and translation. However, the rotation and translation required to bring a second side to coincidence necessarily destroys the coincidence of the first.

The orientation of the optimal plane for two triclinic lattices may be estimated by applying the two-dimensional lattice theory to the normalized axial plane projections: *h* and *l* are given, respectively, by the indices (*h*10) and (01*l*). However, this procedure assumes the constrained lattice rotations of the two-dimensional projections rather than the actual lattice rotation appropriate to (*hkl*), and therefore yields only approximate orientations.

In the present theory, the orientation of optimal phase boundaries is predicted by minimizing the area misfit between normalized equivalent (*hkl*) planes in two related lattices. Area misfit is given by $P = |\epsilon_{11}| + |\epsilon_{22}|$, where, ϵ_{ij} is the two-dimensional strain tensor, formed from five linear strains (the sides of the reference triangle, Fig. 3, and the bisectors of its two largest enclosed angles) computed from the strain-free unit–cell parameters. Area misfit is minimized by inspection, using computer program EPLAG. Strain calculations are made sequentially at grid points on a hemisphere about the Y–axis. Grid points are defined by the spherical coordinates (D,E), where D is a counterclockwise

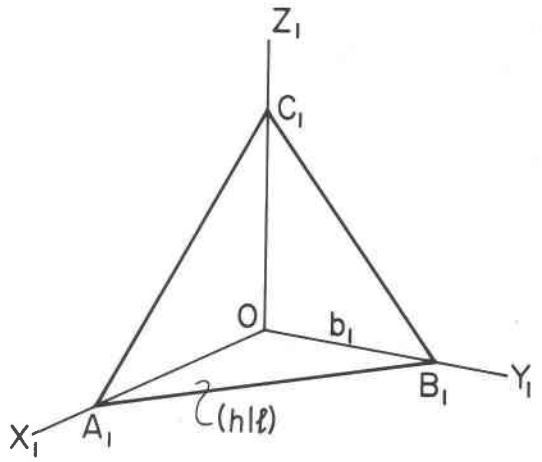

Fig. 3. Reference triangle ABC common to lattices of two intergrown phases.

rotation about the Y–axis (D = 0 in the b,c* plane) and E is a clockwise rotation about an axis normal to the Y–axis and (90 + D)° from c* (E = 0 in the a*,c* plane). Each grid point locates the stereographic pole of an interface plane. The output can be displayed in contoured stereographic projection. Thus the present approach yields the orientations of all planes of low area misfit (not just the optimal one) ranked relative to the quantitative parameter *P*, and permits a visual impression of the variation in misfit in the immediate vicinity of each pole.

EPLAG does not give precise values for lattice rotation, since this would require additional minimization of area misfit by rotation *about* the pole of the optimal (*hkl*) plane. Knowledge of the lattice rotation is not required here in the calculation of optimal phase–boundary orientation as it is in the *0*–lattice theory (Bollmann and Nissen, 1968; Bollman, 1967, 1970). Recognition of the equivalence of the reference triangle in both lattices reduces lattice rotation to a passive role. However, the magnitude of it may be estimated semiquantitatively from the angles subtended by the pole of the optimal plane to the respective crystallographic axis.

The grid interval in EPLAG can be adjusted to the requirements of any particular problem. An interval of 5° is convenient for most reconnaissance work and, with interpolation between grid points, was entirely adequate for study of feldspar mineral intergrowths (below).

EPLAG precisely reproduces the orientation and lattice rotation calculated with the two-dimensional theory for the planes of coincidence in the augite–pigeonite and augite–magnetite intergrowths discussed in the previous section. This is a necessary

first step toward establishing the correctness of the present approach, and is reinforced by the favorable agreement with the observed orientation of feldspar intergrowths reported in the following section.

Coherent elastic strain energy is calculated with a modified version of EPLAG by setting elastic strain components equal to the corresponding principal two-dimensional strains. Stress components outside of the plane of the interface are not set to zero as in the procedure of Willaime and Brown (1974), although the quantitative effects of this modification are rather trivial.

Application to feldspar mineral intergrowths

Feldspars are triclinic and monoclinic framework aluminosilicate phases belonging essentially to two separate solid solution series; (a) plagioclase–$Na_{1-x}Ca_xAl_{1+x}Si_{3-x}O_8$, with albite (Ab, $NaAlSi_3O_8$) and anorthite (An, $CaAl_2Si_2O_8$) end-members; and (b) alkali feldspar–$K_{1-x}Na_xAlSi_3O_8$, with orthoclase (Or, $KAlSi_3O_8$) and albite end-members. Lamellar and lamellar-like intergrowths, mostly resulting from phase-separation processes, are an important diagnostic and genetic characteristic, and have been extensively studied (Smith, 1974). The classification of Willaime and Brown (1974) is adopted in the present study.

(a) Plagioclase

Ordering in triclinic plagioclase solid solutions is complicated by the low mobility of the tetrahedrally coordinated cations, Si and Al. An intimate modulation of end-member components (*e*–plagioclase superstructure) and three separate and compositionally distinct lamellar intergrowths (i. peristerite, ~An2 with ~An25; ii. Bøggild, ~An48 with ~An58; and, iii. Huttenlocher, ~An70 with ~An95) exist in natural phases.

In a previous study with EPLAG (Fleet, 1981), it was shown that the computed minima for lattice misfit and coherent elastic strain energy for albite–intermediate plagioclase and anorthite–intermediate plagioclase interfaces adequately accounts for the compositional dependence of the orientation of the plane of modulation of the *e*–plagioclase superstructure. This suggests that minimization of interface energy is the dominant factor controlling the shape and orientation of the ordered *domains* of albite and anorthite in the superstructure.

The observed orientations of lamellar intergrowths in plagioclase are summarized in Figure 4: these data include the compilations of Smith (1974) and Willaime and Brown (1974) and an exhaustive survey of more recent literature. Poles to plagioclase lamellae have two distinct spatial distributions; (1) near to [010] (and the zone of **s** vectors, which describe the intermediate plagioclase superstructure, Fleet, 1981), and (2) [010] zone, generally near to [100]. Comparative data for lattice misfit minima and coherent elastic strain energy minima (Table 1; Fig. 4) have been calculated with unit–cell parameters obtained by constructing smoothed unit–cell parameter-composition distributions from the data of Grundy and Brown (1969, 1974), and the room-temperature elastic stiffness coefficients of Ryzhova (1974). The ambient temperatures of the calculated data are within the approximate temperature ranges commonly associated with plagioclase intergrowths (*e.g.* McConnell, 1974).

In view of the complexity of the effects which can perturb real intergrowth boundaries, the agreement between the orientations of the calculated optimal and near-optimal boundaries and the actual intergrowths is very good, and could clearly be improved by arbitrary manipulation of the compositions and ambient temperature of the coexisting phases. Furthermore, for [010] zone intergrowths, the consistent discrepancy between the observed orientations and misfit orientations (which are calculated from the strain-free unit–cell parameters) may be attributable to the topological constraint which required the **b*** vectors in the two intergrown phases in [010] zone peristerite to be coincident (McLaren, 1974). As is expected from the relatively large misfit anisotropy of plagioclase intergrowths (P_{max}/P_{min}, Willaime and Brown, 1974), the calculated minima for coherent elastic strain energy more-or-less correspond to the respective misfit minima. However, the areas of the coherent elastic strain energy minima are much more diffuse (Fig. 4) and, therefore, the minima themselves are less well defined.

(b) Alkali feldspar

Alkali feldspar solid solutions unmix to give perthite intergrowths of K–rich feldspar (K–feldspar) and Na–rich feldspar (Na–feldspar). The effects of ordering of the tetrahedrally coordinated cations, Si and Al, are superimposed on the simple solvus phase relations. High temperature K–feldspar (sanidine, orthoclase) is monoclinic; low temperature K–feldspar (microcline) and Na–feldspar (anorthoclase, high and low albite) are triclinic.

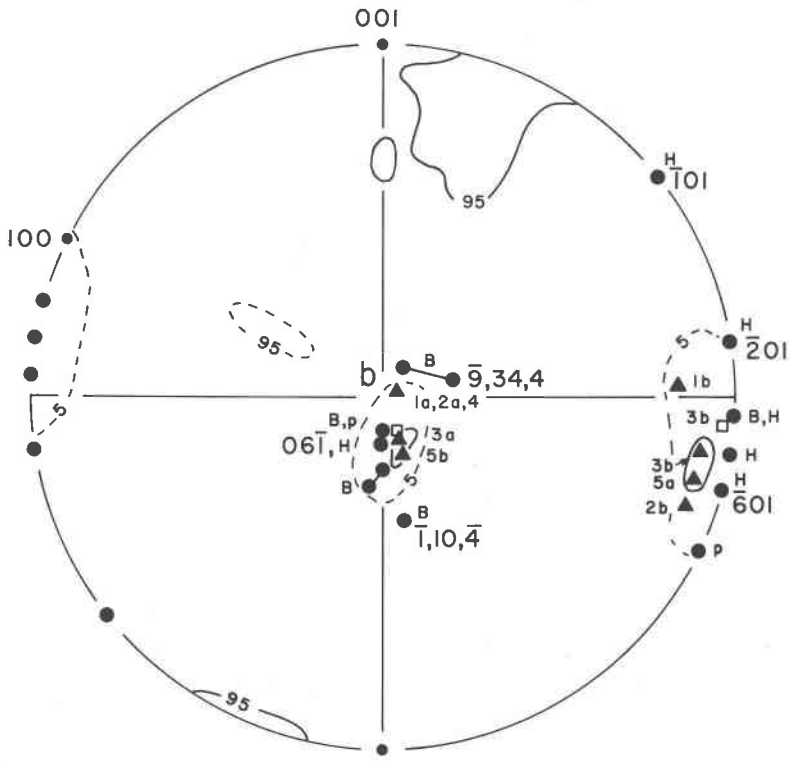

Fig. 4. Orientation of lamellar intergrowths in plagioclase: stereographic projection; circles, observed; p, peristerite; B, Bøggild; H, Huttenlocher; triangles, lattice-misfit minima; squares, coherent elastic strain energy minima; continuous/broken lines are contours of relative percent lattice misfit/strain energy for intergrowth No. 3; labels on calculated data refer to Table 1.

Willaime and Brown (1974) recognized four crystallographically and morphologically distinct groups of perthite:

(1) normal perthite. Spinodally and homogeneously unmixed lamellae, film, vein and patch perthite oriented near $(\bar{6}01)$, $(\bar{8}01)$: (scale; crypto-, micro- and macroperthite).

(2) braid perthite. Intersecting pairs of $(hk\bar{l})$ and $(h\bar{k}\bar{l})$ lamellae of Na–feldspar forming a braided pattern parallel to (100). The $(1\bar{1}0)$, (110) combination is most common, but $(86\bar{1})$, $(8\bar{6}\bar{1})$ and $(3\bar{2}0)$, (320) are also frequent. Albite twin lamellae have a preferred orientation in Na–feldspar (the major phase); each lamellar orientation is associated with a particular twin orientation: (micro- and macroperthite).

(3) diagonal association perthite. Lozenge-shaped units of diagonally-associated microcline (Smith and MacKenzie, 1959) in a zig-zag pattern parallel to $(63\bar{1})$,$(6\bar{3}\bar{1})$ or $(66\bar{1})$, $(6\bar{6}\bar{1})$ (Willaime and Brown, 1974). Each lozenge orientation appears to be associated with a particular diagonally-associated twin orientation: (cryptoperthite).

(4) plate perthite. Irregular plate-like lamellae of untwinned low albite approximately parallel to (011) of untwinned microcline (Laves and Soldatos, 1962). Individual plates may consist of smaller plates arranged *en echelon* (Smith, 1974): (macroperthite).

The observed orientations of perthite intergrowths are summarized in Figures 5, 6, and 7. Comparative data for lattice misfit minima and coherent elastic strain energy minima have been calculated with room-temperature unit–cell parameters from the compilation of Willaime and Brown (Table 1, 1974) and from smoothed unit–cell parameter-composition distributions from the data of Wright and Stewart (1968), and the room-temperature elastic stiffness coefficients from the compilation of Willaime and Brown (Table 2, 1974). The calculated orientations reported in Table 1 and Figures 5, 6, and 7 have been selected from a large number of individual calculations made to estimate the effects of composition, structural state, topological constraints, anisotropic elasticity and misfit parameters on perthite intergrowth orientation. The relevance of these data to each group of perthite intergrowth is summarized below:

Table 1. Calculated phase-boundary orientations for feldspar intergrowths

Feldspar Intergrowth	No.		Model Intergrowth*	Data†	Lattice Misfit Minima h	k	ℓ	Strain Energy Minima h	k	ℓ	P_{max}/P_{min}
Plagioclase Peristerite	1	a	L Ab(An0)-Olig(An20),450°C	1	$\bar{1}$	19	0	$\bar{1}$	19	0	5.15
		b			$\bar{12}$	3	5	$\bar{10}$	3	6	4.62
	2	a	L Ab(An0)-Olig(An20),750°C	1	0	1	0				3.47
		b			8	1	1				3.27
Bøggild	3	a	And(An45)-Lab(An55),450°C	1	$\bar{1}$	17	$\bar{2}$	$\bar{1}$	17	$\bar{2}$	8.36
		b			$\bar{15}$	2	3	$\bar{15}$	1	5	7.34
	4		And(An45)-Lab(An55),750°C	1	$\bar{1}$	19	0				4.32
Huttenlocher	5	a	Byt(An70)-An(An90),450°C	1	$\bar{15}$	2	3	$\bar{1}$	16	$\bar{2}$	8.59
		b			$\bar{1}$	16	3	7	1	2	8.37
Alkali Feldspar Normal Perthite, and	1		San(Or50)-San(Or25)	2	9	0	$\bar{1}$	9	0	$\bar{1}$	4.09
	2	a	San(Or50)-Anorth(Or25)	2	6	13	$\bar{1}$	0	18	1	2.55
		b			7	3	11	0	1	3	2.53
		c			5	1	4	2	3	0	2.43
	2Aa		San(Or50)-Anorth(Or25,A)	2	6	13	1				2.55
		b			7	3	$\bar{11}$				2.53
	3	a	San(1)-H Ab(4)	3	$\bar{11}$	3	5				2.50
		b			4	5	$\bar{1}$				2.40
	3Aa		San(1)-H Ab(4,A)	3	11	3	5				2.50
		b			4	5	1				2.40
	4	a	Int Mic(8)-H Ab(4)		7	11	2				2.72
		b			$\bar{13}$	2	5				2.70
Diagonal Association Perthite	5	a	Int Mic(8)-Int Ab(12)	3	$\bar{10}$	4	5				2.35
		b			8	9	3				2.33
	5Aa		Int Mic(8,A)-Int Ab(12)	3	11	3	6				2.32
		b			7	12	$\bar{1}$				2.31
	6		Max Mic(9)-L Ab(12A)(W&B)	3	11	8	0	11	8	$\bar{1}$	6.46
Braid Perthite	1	a	Or(7)-L Ab(13)	3	8	11	$\bar{2}$	$\bar{2}$	2	1	2.41
		b			11	2	7				2.39
	1Aa		Or(7)-L Ab(13,A)	3	8	11	1				2.41
		b			6	1	3				2.39
	2	a	Int Mic(8)-L Ab(14)	3	9	9	$\bar{2}$				2.32
		b			2	1	$\bar{1}$				2.31
	2Aa		Int Mic(8)-L Ab(14,A)	3	7	12	0				2.63
		b			6	1	3				2.52
	3	a	Or-L Ab(B&N)	4	8	11	$\bar{2}$				2.41
		b			11	3	6				2.37
Plate Perthite	1	a	Max Mic(9)-L Ab(14)	3	4	5	$\bar{1}$	0	9	1	2.47
		b			$\bar{11}$	3	5	12	7	1	2.47
		c						15	2	3	
		d						0	1	3	
	1A		Max Mic(9)-L Ab(14,A)	3	6	14	1				3.15

* Abbreviations: L,low; H,high; Ab,albite; Olig,oligoclase; And,andesine; Lab, labradorite; Byt,bytownite; An,anorthite; San,sanidine; Anorth,anorthoclase; Int,intermediate; Max,maximum; Mic,microcline; (W&B),Willaime and Brown; (B&N),Bollmann and Nissen; A, albite twin-related unit-cell parameters with $\alpha'=180-\alpha$, $\gamma'=180-\gamma$.

† Source of unit-cell data: 1. Grundy and Brown (1969; 1974), see text; 2. Wright and Stewart (1968), see text; 3. Willaime and Brown (1974, Table 1); 4. Bollmann and Nissen (1968).

(1) normal perthite. The optimal boundary for the coexisting monoclinic alkali feldspars Or50–Or25, representing the early stages of alkali feldspar unmixing, is in good agreement with the orientation of cryptoperthite lamellae (Table 1; Fig. 5). However, the calculated boundaries for coexisting strain-free monoclinic K–feldspar–triclinic Na–feldspar and triclinic K–feldspar–triclinic Na–feldspar are inclined by 40 to 50° to [010]. Clearly, the phase boundary of cryptoperthite intergrowths in which Na–feldspar is triclinic are constrained to lie in the [010] zone, near to $(\bar{6}01)$. As in [010] zone peristerite, there is a topological constraint which requires the **b*** vectors in the two intergrown phases to be coincident. This is manifest in anomalous unit–cell parameters (Smith, 1974). The calculated minimum for coherent elastic strain energy for sanidine–sanidine unit–cell parameters corresponds to the respective misfit minimum, as expected from the earlier studies of Willaime and Brown (1974), Robin (1974) and Tullis and Yund (1979). However, for sanidine–anorthoclase unit–cell parameters the strongest minimum of coherent elastic strain energy is near [010]!

(2) braid perthite. Optimal and near-optimal boundary orientations for coexisting orthoclase–low albite are in good agreement with one of the lamellar orientations in each of the pairs of intersecting lamellae reported for braid perthite (Table 1; Fig. 6). The symmetry relations of the two lamellae in each pair suggest they are related by the albite twin operation [(010) twin plane], and this is confirmed by minima calculated with Na–feldspar unit–cell parameters modified by $\alpha' = 180 - \alpha$, $\gamma' = 180 - \gamma$ (Fig. 6). The symmetry relationship of the calculated orientations for albite–twinned lamellae only exists when the K–feldspar phase is monoclinic. It deteriorates for intermediate microcline (Fig. 6), and is nonexistent for maximum microcline. Thus the present misfit theory clearly indicates that braid perthite develops through equilibration (unmixing or replacement) between orthoclase and low albite, and that the albite twin lamellae were present during this process. The present results on the applicability of optimal phase boundary theory to braid perthite directly contradict the conclusions of Willaime and Brown (1974). Furthermore, calculated minima for coherent elastic strain energy are only in fair agreement with the observed lamellar orientations (Fig. 6).

(3) diagonal association perthite. Diagonal association perthite appears to be a maturation feature of Na–rich moonstone and anorthoclase (Willaime, Brown and Gandais, 1976). Optimal boundaries for appropriate combinations of sanidine or intermediate microcline and high or low albite are only in fair to poor agreement with the *reported* observed interface orientations (Fig. 4). However, the latter appear to have been estimated from transmission electron microscope (TEM) micrographs of (010) cleavage fragments, and may have been rounded to be consistent with the calculated boundaries of Willaime and Brown (1974). The precise measurements of Lorimer and Champness (1973) actually correspond to $(99\bar{2})$, which is in excellent agreement with the present optimal boundaries, and $(\bar{9}92)$, which, following the previous analysis of braid perthite lamellae, is probably twin-related to $(99\bar{2})$. Logically, $(\bar{9}92)$ should be related through diagonally associated twinning to $(99\bar{2})$, and the data for

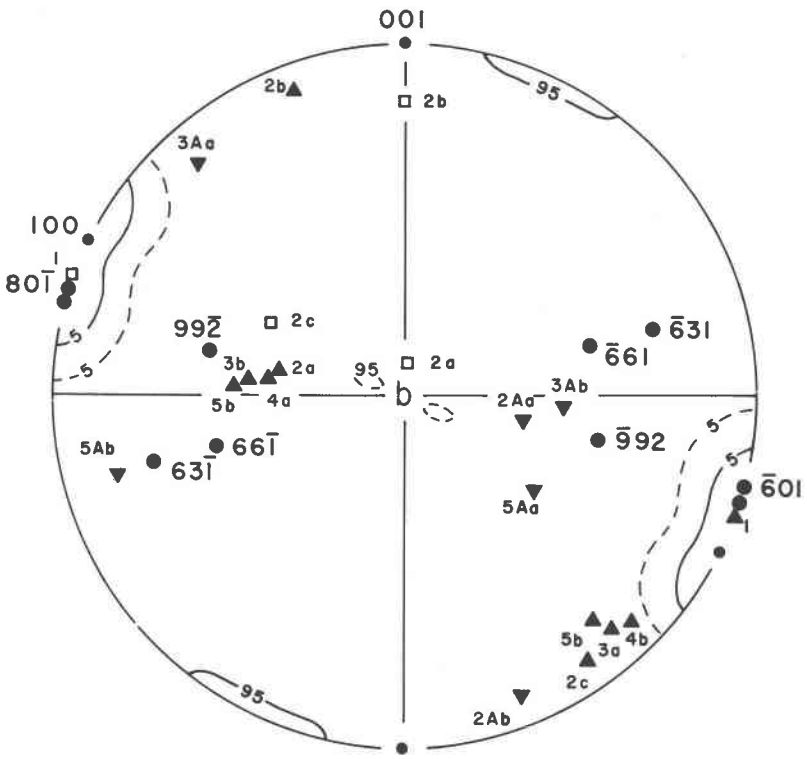

Fig. 5. Orientation of normal perthite and diagonal association perthite intergrowths: symbols as in Fig. 4; contours are for intergrowth No. 1.

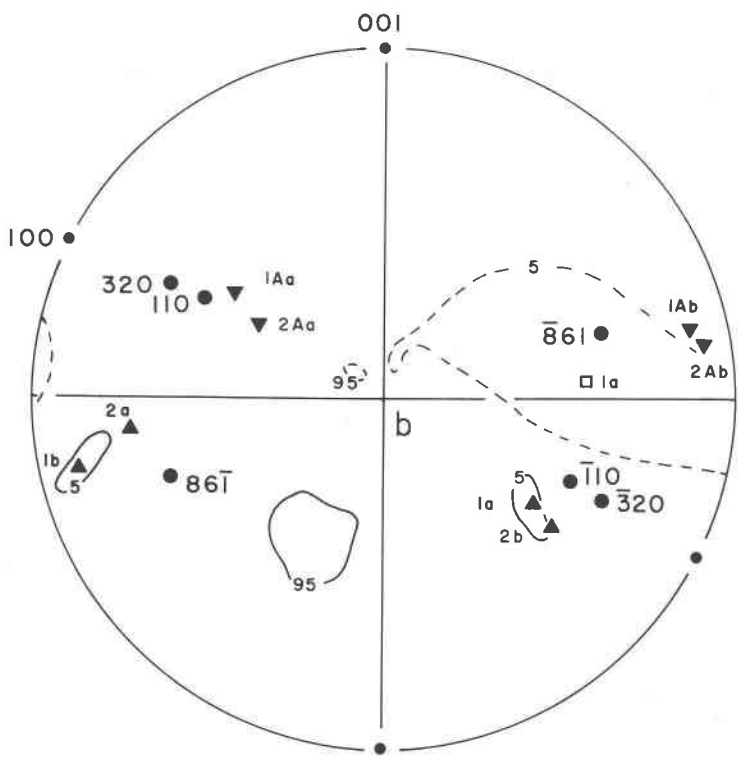

Fig. 6. Orientation of braid perthite intergrowths: symbols as in Fig. 4; contours are for intergrowth No. 1.

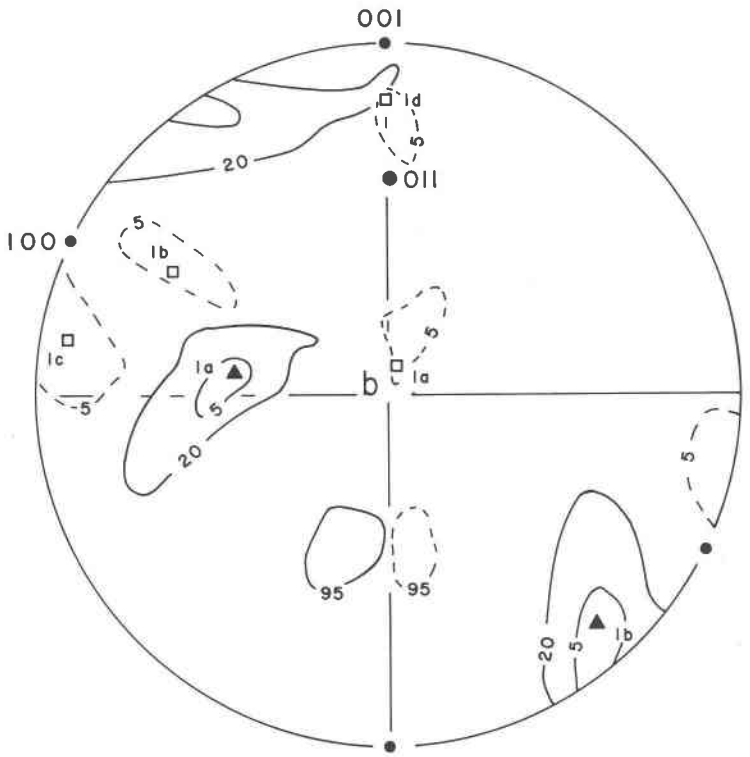

Fig. 7. Orientation of plate perthite intergrowth, compared to lattice misfit and coherent elastic strain energy data calculated for maximum microcline-low albite intergrowth: symbols as in Fig. 4.

coexisting intermediate microcline–intermediate albite (Fig. 4) tend to support this supposition. Alternatively, it is possible that the symmetry-related interface pairs are related to preexisting *coarse* albite twin lamellae in the Na–feldspar: this would result in a more regular intergrowth texture. However, the present analysis indicates quite positively that the fine albite twin lamellae in the Na–feldspar *post-date* intergrowth development. This is in agreement with Lorimer and Champness (1973), and contradicts the theory of Willaime and Brown (1974). Calculated minima for coherent elastic strain energy are only in fair agreement with the observed orientations (as indicated above), but *differ* from the equivalent data of Willaime and Brown (1974): data for maximum microcline–albite–twinned (equivalent monoclinic) low albite are included in Table 1 for comparison.

(4) plate perthite. The optimal boundary for coexisting maximum microcline–low albite does not agree with the orientation of plate perthite (Fig. 7). However, the near-optimal boundary $(\bar{1}\bar{1},3,\bar{5})$, which is associated with an area of minimum misfit extending to the [100] zone, is in closer agreement. For coexisting sanidine–anorthoclase the equivalent near-optimal boundary itself is in fair agreement with the observed orientation (Fig. 5). However, the discrepancy between the calculated and observed data is more likely to be attributable to uncertainty in the morphology and orientation of the intergrowth, and to its coarse nature. Minima for coherent elastic strain energy have a distinctively different spatial distribution to the misfit minima (Willaime and Brown, 1974; Figs. 7 and 5).

Discussion

Previous theories and concepts

The *0*-lattice theory (Bollmann, 1967, 1970) is rigorously derived for two identical lattices differing only in orientation and (possibly) origin. Hence it is essentially only applicable to subgrain boundaries and to grain boundaries between grains of the same phase. Bollmann and Nissen (1968) applied *0*-lattice theory to alkali feldspar intergrowths by introducing a minimization parameter for lattice misfit, $P = (b_1/d_1)^2 + (b_2/d_2)^2$, where, b_1 and b_2 are Burgers vectors for dislocation arrays of spacings d_1 and d_2.

This revised *0*-lattice theory has similarities to the present misfit theory, but it is not equivalent to it: the optimal and near-optimal boundary orientations for the intergrowth example used by Bollmann and Nissen (1968) differ by about 16° and 10°, respectively (Table 1).

For intergrowths between cubic alloy phases lattice misfit is isotropic, and therefore there is no tendency for lattice rotation to minimize it. Fine scale precipitates in such systems are generally oriented parallel to elastically soft planes (Cahn, 1968), and TEM studies confirm that this phenomenon is related to minimization of coherent elastic strain energy. However, the existence of *intersecting* lamellae and high-resolution TEM studies show quite convincingly that coherency stresses must be very local, and that lattice strain is relaxed within a few unit cells of the interface. Presumably this is accommodated by shear stresses outside of the interface plane and by dislocations.

Willaime and Brown (1974) generalized the conclusion of Cahn (1968) to include intergrowths between phases of non-cubic symmetry, arguing that all juxtaposed lattices are strained to coherence at the time phase-boundary orientation is defined. However, the present EPLAG data suggest that the observed orientations of feldspar intergrowths are much more consistent with minimization of lattice misfit than with minimization of coherent elastic strain energy. Very few feldspar intergrowths are properly coherent under laboratory conditions, and semicoherency effects are usually referable to topological constraints rather than to coherency constraints imposed by interface planes. The only feldspar intergrowth for which the coherent elastic strain energy model gives better agreement that the simple misfit theory is plate perthite, which, ironically, is coarse in scale and has a pronounced lattice rotation (Laves and Soldatos, 1962).

Intergrowths of chain-silicates (Robinson *et al.*, 1977; Fleet *et al.*, 1980) exhibit a lattice rotation and a phase-boundary orientation that are precisely reproduced by two-dimensional lattice misfit theory. There is no doubt that the lattice misfit at the phase boundary has been reduced by lattice rotation. Coincident phase boundaries do not directly negate the general applicability of the coherent elastic strain energy theory (since coherent elastic strain energy is also zero at coincidence), but they do demonstrate that the concepts of lattice coherence and structural continuity, which have emerged from study of intergrowths between cubic alloy phases, have to be modified for intergrowths between phases of non-cubic symmetry.

Optimal phase boundaries

It seems clear from the foregoing discussion that minimization of lattice misfit is the dominant factor controlling the orientation of phase boundaries in crystalline solids of low symmetry. The available evidence suggests that the contribution of anisotropic elasticity is relatively insignificant except when the lattice misfit is essentially isotropic. Hence the phase boundaries of intergrowths will, in general, represent optimal boundaries, except where special circumstances permit coincident boundaries with no residual coherency stresses.

It is expected that structural accommodation at optimal phase boundaries is facilitated by local coherency stresses, dislocations and stacking faults. The contribution of local coherency stresses should decrease with coarsening. In the early stages of phase separation it may be a dominant factor. However, the calculation of the total energy contribution associated with such stresses is fraught with problems. In particular, the effects of strain relaxation and of topological constraints, which introduce elastic strains outside of the plane of the phase boundary, have to be taken into account.

Topological constraints

The two principal perturbing factors in the reproduction of phase-boundary orientation with optimal phase-boundary theory are topological constraints in fine-scale intergrowths and coarsening. Neither may be quantitatively compensated. The effects of coarsening are self-evident, since it leads to a reduction in specific surface area.

Topological constraints may be expected in intergrowths of isomorphous or pseudo-isomorphous phases whose crystal structures contain infinite chains, sheets or frameworks of strongly bonded atoms. Coincidence vectors arise through the requirement to equalize bond distances in *shared* or *equivalent* structural features. Such features are not necessarily parallel to optimal planes calculated from the strain-free unit-cell parameters. It has been noted previously that the **b*** vectors in peristerite and cryptoperthite intergrowths tend to be coincident. Anomalies also exist in chain-silicate intergrowths. Hornblende lamellae in augite (Smith, 1977) and biopyribole intergrowths (Veblen and Buseck, 1980) are oriented parallel to (010), with [100] and [001] vectors coincident, rather than the

[010] zones as suggested by optimal phase boundary theory.

Acknowledgments

Thanks go to Milan Rieder for locating a programming error in EPLAG, and to Richard A. Yund for reviewing the manuscript. This study was supported by a Natural Sciences and Engineering Council of Canada operating grant.

References

Bollmann, W. (1967) On the geometry of grain and phase boundaries I. General theory. Philosophical Magazine, 16, 363–383.

Bollmann, W. (1970) Crystal Defects and Crystalline Interfaces. Springer-Verlag, Berlin.

Bollmann, W. and Nissen, H. U. (1968) A study of optimal phase boundaries: The case of exsolved alkali feldspars. Acta Crystallographica, A24, 546–557.

Cahn, J. W. (1968) Spinodal decomposition. Transactions of the Metallurgical Society of AIME, 242, 166–180.

Fleet, M. E. (1981) The intermediate plagioclase structure: An explanation from interface theory. Physics and Chemistry of Minerals, 7, 64–70.

Fleet, M. E., Bilcox, G. A. and Barnett, R. L. (1980) Oriented magnetite inclusions in pyroxenes from the Grenville province. Canadian Mineralogist, 18, 89–99.

Grundy, H. D. and Brown, W. L. (1969) A high temperature X-ray study of the equilibrium forms of albite. Mineralogical Magazine, 37, 156–172.

Grundy, H. D. and Brown, W. L. (1974) A high-temperature X-ray study of low and high plagioclase feldspars. In W. S. MacKenzie and J. Zussman, Eds., The Feldspars, p. 162–173. Proceedings of NATO Advanced Study Institute, University Press, Manchester, England.

Jaffe, H. W., Robinson, Peter and Tracy, R. J. (1975) Orientation of pigeonite exsolution lamellae in metamorphic augite: correlation with composition and calculated optimal phase boundaries. American Mineralogist, 60, 9–28.

Laves, F. and Soldatos, K. (1962) Plate perthite, a new perthite intergrowth in microcline single crystals, a recrystallization product. Zeitschrift für Kristallographie, 117, 218–226.

Lorimer, G. W. and Champness, P. E. (1973) The origin of the phase distribution in two perthitic alkali feldspars. Philosophical Magazine, 28, 1391–1403.

McConnell, J. D. C. (1974) Electron-optical study of the fine structure of a schiller labradorite. In W. S. MacKenzie and J. Zussman, Eds., The Feldspars, p. 478–490. Proceedings of NATO Advanced Study Institute, University Press, Manchester, England.

McLaren, A. C. (1974) Transmission electron microscopy of the feldspars. In W. S. MacKenzie and J. Zussman, Eds., The Feldspars, p. 378–423. Proceedings of NATO Advanced Study Institute, University Press, Manchester, England.

Robin, P.-Y. F. (1974) Stress and strain in cryptoperthite lamellae and the coherent solvus of alkali feldspars. American Mineralogist, 59, 1299–1318.

Robin, P.-Y. F. (1979) Angular relationships between host and exsolution lamellae and the use of the Mohr circle. American Mineralogist, 62, 127–131.

Robinson, Peter, Jaffe, H. W., Ross, M. and Klein, C. (1971) Orientation of exsolution lamellae in clinopyroxenes and clinoamphiboles: consideration of optimal phase boundaries. American Mineralogist, 56, 909–939.

Robinson, Peter, Ross, M., Nord, G. L., Smyth, J. R. and Jaffe, H. W. (1977) Exsolution lamellae in augite and pigeonite: fossil indicators of lattice parameters at high temperature and pressure. American Mineralogist, 62, 857-873.

Ryzhova, T. V. (1964) Elastic properties of plagioclase. Bulletin of the Academy of Sciences of USSR–Izvestia Geophysics, 7, 633–635.

Smith, J. V. (1974) Feldspar Minerals, vols. I and II. Springer-Verlag, Berlin.

Smith, J. V. and MacKenzie, W. S. (1959) The alkali feldspars. V. The nature of orthoclase and microcline perthites, and observations concerning the polymorphism of potassium feldspar. American Mineralogist, 44, 1169–1186.

Smith, P. P. K. (1977) An electron microscope study of amphibole lamellae in augite. Contributions to Mineralogy and Petrology, 59, 317–322.

Tullis, J. and Yund, R. A. (1979) Calculation of coherent solvi for alkali feldspar, iron-free clinopyroxene, nepheline-kalsilite, and hematite-ilmenite. American Mineralogist, 64, 1063–1074.

Veblen, D. R. and Buseck, P. R. (1980) Microstructures and reaction mechanisms in biopyriboles. American Mineralogist, 65, 599–623.

Willaime, C. and Brown, W. L. (1974) A coherent elastic model for the determination of the orientation of exsolution boundaries: Application to the feldspars. Acta Crystallographica. A30, 316–331.

Willaime, C., Brown, W. L. and Gandais, M. (1976) Physical aspects of exsolution in natural alkali feldspars. In H.-R. Wenk, Ed., Electron Microscopy in Mineralogy, p. 248–257. Springer-Verlag, Berlin.

Wright, T. L. and Stewart, D. B. (1968) X-ray and optical study of alkali feldspar. I. Determination of composition and structural state from refined unit-cell parameters and 2V. American Mineralogist, 53, 38–87.

Manuscript received, August 13, 1981;
accepted for publication, May 10, 1982.